Supplement of

Molecular composition and volatility of multi-generation products formed from isoprene oxidation by nitrate radical

Rongrong Wu et al.

Correspondence to: Thomas F. Mentel (t.mentel@fz-juelich.de)

Table S1: Possible permutation scheme for dimers formed through RO_2 + $R'O_2$ reactions. Molecular formulas presented in dark colors (colored by isomers) are compounds detected by CIMS in this study, while those in light grey were not.

$C_5H_8NO_x$ $C_5H_8NO_x$	O_5	O_6	O_7	O_8	O_9
O_5	$C_{10}H_{16}N_2O_8$				
O_6	$C_{10}H_{16}N_2O_9$	$C_{10}H_{16}N_2O_{10}$			
O_7	$C_{10}H_{16}N_2O_{10}$	$C_{10}H_{16}N_2O_{11}$	$C_{10}H_{16}N_2O_{12}$		
O_8	$C_{10}H_{16}N_2O_{11}$	$C_{10}H_{16}N_2O_{12}$	$C_{10}H_{16}N_2O_{13}$		
O_9	$C_{10}H_{16}N_2O_{12}$	$C_{10}H_{16}N_2O_{13}$	$C_{10}H_{16}N_2O_{14}$		
O_{10}	$C_{10}H_{16}N_2O_{13}$	$C_{10}H_{16}N_2O_{14}$	$C_{10}H_{16}N_2O_{15}$		
O_{11}	$C_{10}H_{16}N_2O_{14}$	$C_{10}H_{16}N_2O_{15}$	$C_{10}H_{16}N_2O_{16}$		
O_{12}	$C_{10}H_{16}N_2O_{15}$	$C_{10}H_{16}N_2O_{16}$	$C_{10}H_{16}N_2O_{17}$		

$C_5H_8NO_x$ $C_5H_9N_2O_y$	O_5	O_6	O_7	O_8	O_9
O_9	$C_{10}H_{17}N_3O_{12}$	$C_{10}H_{17}N_3O_{13}$	$C_{10}H_{17}N_3O_{14}$	$C_{10}H_{17}N_3O_{15}$	$C_{10}H_{17}N_3O_{16}$
O_{10}	$C_{10}H_{17}N_3O_{13}$	$C_{10}H_{17}N_3O_{14}$	$C_{10}H_{17}N_3O_{15}$	$C_{10}H_{17}N_3O_{16}$	$C_{10}H_{17}N_3O_{17}$
O_{11}	$C_{10}H_{17}N_3O_{14}$	$C_{10}H_{17}N_3O_{15}$	$C_{10}H_{17}N_3O_{16}$	$C_{10}H_{17}N_3O_{17}$	$C_{10}H_{17}N_3O_{18}$
O_{12}	$C_{10}H_{17}N_3O_{15}$	$C_{10}H_{17}N_3O_{16}$	$C_{10}H_{17}N_3O_{17}$	$C_{10}H_{17}N_3O_{18}$	$C_{10}H_{17}N_3O_{19}$
O_{13}	$C_{10}H_{17}N_3O_{16}$	$C_{10}H_{17}N_3O_{17}$	$C_{10}H_{17}N_3O_{18}$	$C_{10}H_{17}N_3O_{19}$	$C_{10}H_{17}N_3O_{20}$
O_{14}	$C_{10}H_{17}N_3O_{17}$	$C_{10}H_{17}N_3O_{18}$	$C_{10}H_{17}N_3O_{19}$	$C_{10}H_{17}N_3O_{20}$	$C_{10}H_{17}N_3O_{21}$
O_{15}	$C_{10}H_{17}N_3O_{18}$	$C_{10}H_{17}N_3O_{19}$	$C_{10}H_{17}N_3O_{20}$	$C_{10}H_{17}N_3O_{21}$	$C_{10}H_{17}N_3O_{22}$
O_{16}	$C_{10}H_{17}N_3O_{19}$	$C_{10}H_{17}N_3O_{20}$	$C_{10}H_{17}N_3O_{21}$	$C_{10}H_{17}N_3O_{22}$	$C_{10}H_{17}N_3O_{23}$

$C_5H_9N_2O_y$ $C_5H_9N_2O_y$	O_9	O_{10}	O_{11}	O_{12}	O_{13}
O_9	$C_{10}H_{18}N_4O_{16}$				
O_{10}	$C_{10}H_{18}N_4O_{17}$				
O_{11}	$C_{10}H_{18}N_4O_{18}$				
O_{12}	$C_{10}H_{18}N_4O_{19}$				
O_{13}	$C_{10}H_{18}N_4O_{20}$				
O_{14}	$C_{10}H_{18}N_4O_{21}$				
O_{15}	$C_{10}H_{18}N_4O_{22}$				
O_{16}	$C_{10}H_{18}N_4O_{23}$				

Table S2: Ions observed in the gas phase by CIMS and proposed possible products from isoprene oxidation by NO_3

No.	Molecular formula	Molecular weight	Observed m/z (-)	Proposed structure
1	$C_4H_7NO_5$	149	228, 230	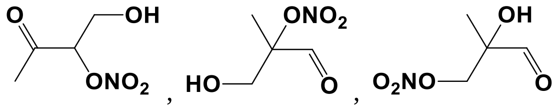
2	$C_5H_7NO_4$	145	224, 226	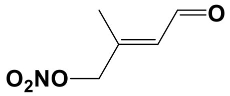
3	$C_5H_7NO_5$	161	240, 242	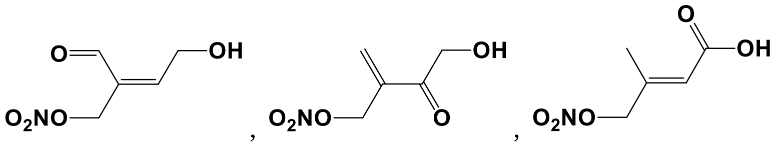
4	$C_5H_7NO_6$	177	256, 258	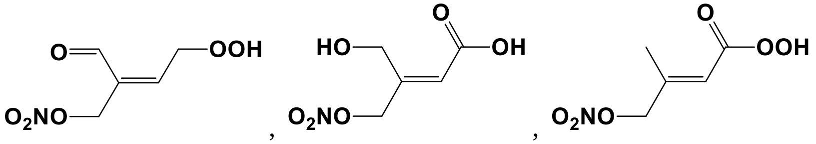
5	$C_5H_7NO_7$	193	272, 274	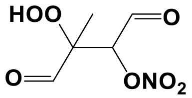
6	$C_5H_9NO_4$	147	226, 228	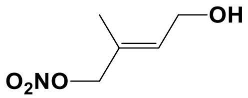
7	$C_5H_9NO_5$	163	242, 244	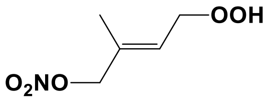
8	$C_5H_9NO_6$	179	258, 260	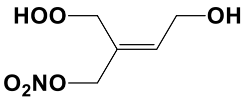

9	$C_5H_9NO_7$	195	274, 276	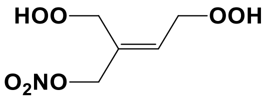 , 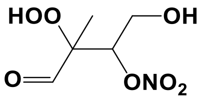
10	$C_4H_6N_2O_7$	194	273, 275	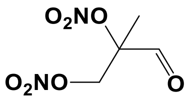 , 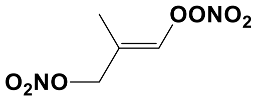
11	$C_5H_6N_2O_8$	222	301, 303	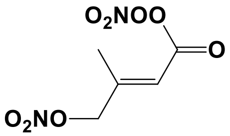 , 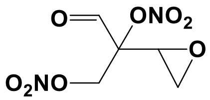 , 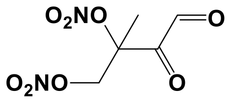
12	$C_5H_8N_2O_7$	208	287, 289	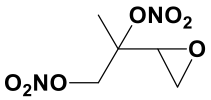 , 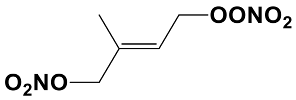
13	$C_5H_8N_2O_8$	224	303, 305	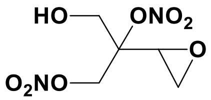 , 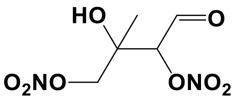
14	$C_5H_8N_2O_9$	240	319, 321	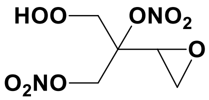 , 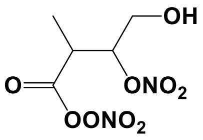 , 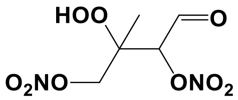 , 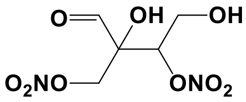
15	$C_5H_8N_2O_{10}$	256	335, 337	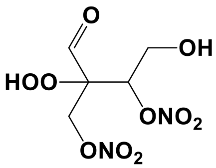 , 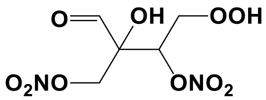 , 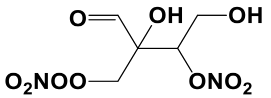 , 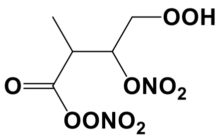

16	$C_5H_{10}N_2O_8$	226	305, 307	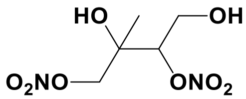
17	$C_5H_{10}N_2O_9$	242	321, 323	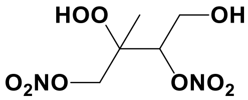 , 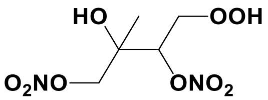
18	$C_5H_{10}N_2O_{10}$	258	337, 339	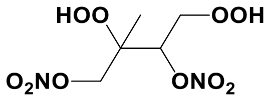 , 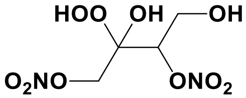
19	$C_5H_9N_3O_{10}$	271	350, 352	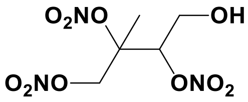
20	$C_5H_9N_3O_{11}$	287	366, 368	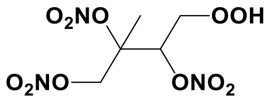 , 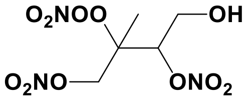
21	$C_5H_9N_3O_{12}$	303	382, 384	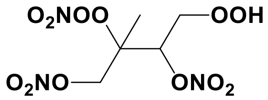 , 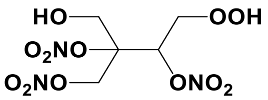
22	$C_{10}H_{16}N_2O_8$	292	371, 373	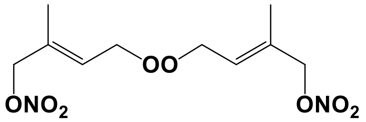
23	$C_{10}H_{16}N_2O_9$	308	387, 389	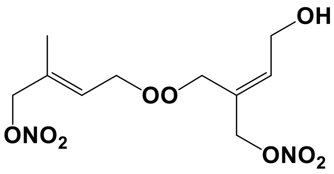
24	$C_{10}H_{16}N_2O_{10}$	324	403, 405	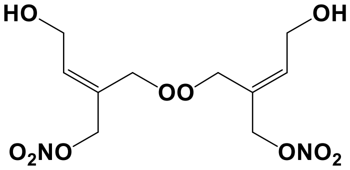 , 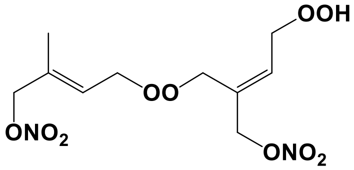 ,

				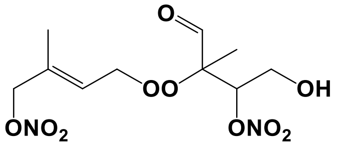
25	$C_{10}H_{16}N_2O_{11}$	340	419, 421	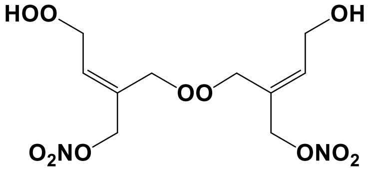 , 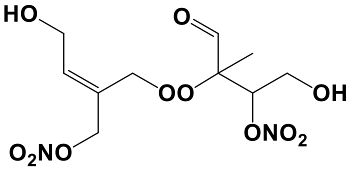 , 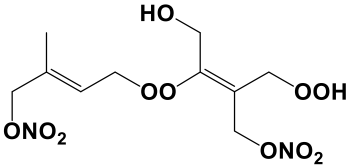
26	$C_{10}H_{16}N_2O_{12}$	356	435, 437	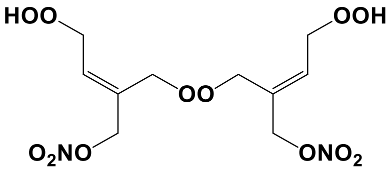 , 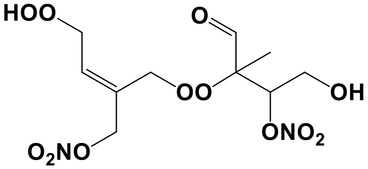 , 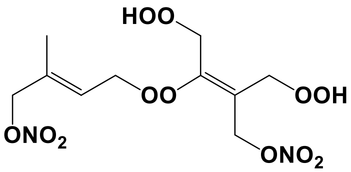 , 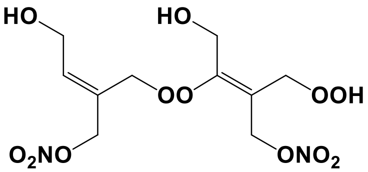 , 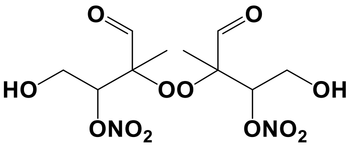
27	$C_{10}H_{16}N_2O_{13}$	372	451, 453	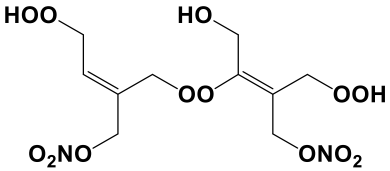 , 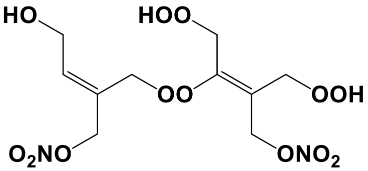 ,

				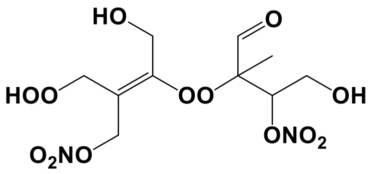
28	$C_{10}H_{17}N_3O_{12}$	371	450, 452	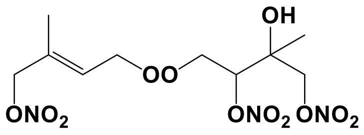 , 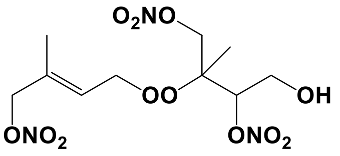
29	$C_{10}H_{17}N_3O_{13}$	387	466, 468	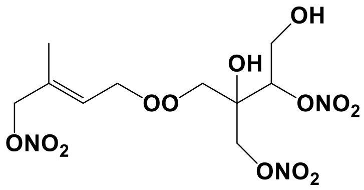 , 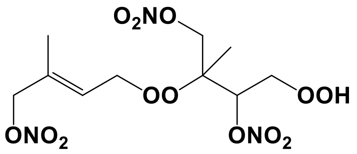 , 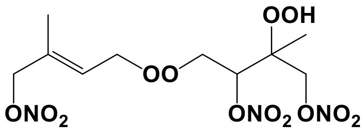 , 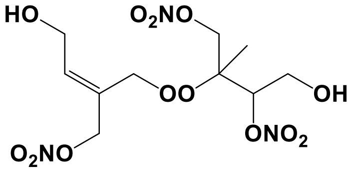
30	$C_{10}H_{17}N_3O_{14}$	403	482, 484	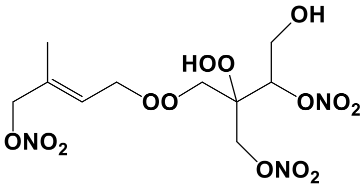 , 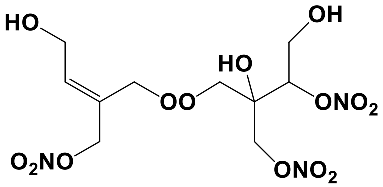 , 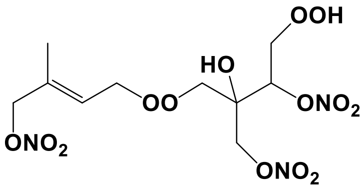 , 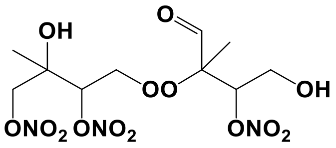

31	$C_{10}H_{17}N_3O_{15}$	419	498, 500	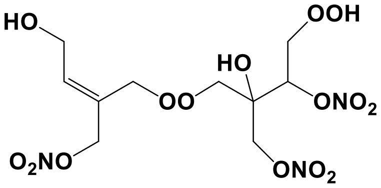, 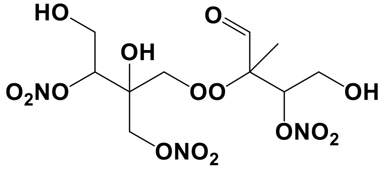, 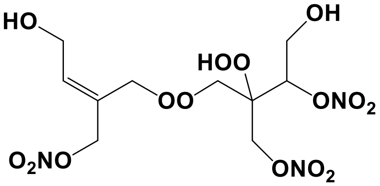
32	$C_{10}H_{17}N_3O_{16}$	435	514, 516	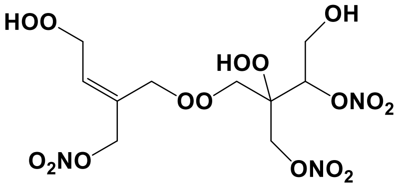, 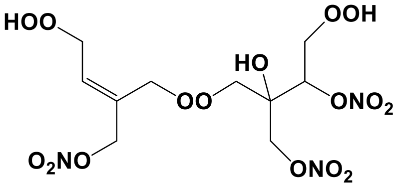, 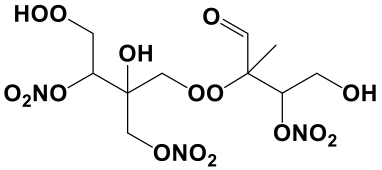, 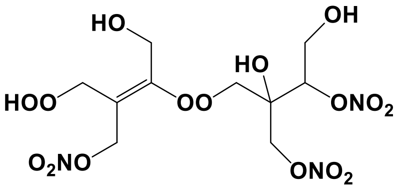

Table S3 lists the wall loss rates of dimers that used for wall-loss correction. Assuming that the dimers undergo irreversible gas-wall partitioning, then the overall wall loss rate of an organic species i ($k_{w,i}$) can be written as Eq. (S1) (Zhang et al., 2015).

$$k_{w,i}=\left(\frac{A}{V}\right)\left(\frac{\alpha_{w,i}\bar{v}_i/4}{\pi\alpha_{w,i}\,\bar{v}_i/8\,(D_iK_e)^{1/2}+1}\right) \tag{S1}$$

where A/V is the surface to volume ratio of the SAPHIR chamber, $\alpha_{w,i}$ is the mass accommodation coefficient of species i onto the chamber wall, $\bar{v}_i$ is the mean thermal speed of species i, D_i is the molecular diffusivity, and K_e is the coefficient of eddy diffusion. D_i varies with molecular weight (MW) and is equal to $D_{CO_2}\times\left(MW_{CO_2}/MW_i\right)$ with D_{CO_2}= 1.38×10-5 m^2 s^{-1} (Zhang et al., 2014). The mean speed of a gas molecule is defined as:

$$\bar{v}_i=\left(\frac{8N_A\kappa T}{\pi MW_i}\right)^{\frac{1}{2}} \tag{S2}$$

where N_A is the Avagadro's number, κ is the Boltzmann constant and T is the temperature.
The value of K_e for the SAPHIR chamber is estimated based on Eq. (S3) (Krechmer et al., 2016):

$$K_e=0.004+\left(5.6\times10^{-3}\right)(V)^{0.74} \tag{S3}$$

In the irreversible partitioning case, the wall loss behavior is governed by the wall accommodation coefficient. $\alpha_{w,i}$ Zhang et al. (2015) observed a strong negative correlation between $\alpha_{w,i}$ and the saturation concentration C_i^*, and they formulated an empirical expression for $\alpha_{w,i}$ as a function of C_i^* based on the measurements:

$$log_{10}\left(\alpha_{w,i}\right)=-0.1919\times log_{10}\left(C_i^*\right)-6.32 \tag{S4}$$

References

Krechmer, J. E., Pagonis, D., Ziemann, P. J., and Jimenez, J. L.: Quantification of gas-wall partitioning in Teflon environmental chambers using rapid bursts of low-volatility oxidized species generated in situ, Environmental science & technology, 50, 5757-5765, 2016.

Zhang, X., Cappa, C. D., Jathar, S. H., McVay, R. C., Ensberg, J. J., Kleeman, M. J., and Seinfeld, J. H.: Influence of vapor wall loss in laboratory chambers on yields of secondary organic aerosol, Proceedings of the National Academy of Sciences, 111, 5802-5807, 2014.

Zhang, X., Schwantes, R., McVay, R., Lignell, H., Coggon, M., Flagan, R., and Seinfeld, J.: Vapor wall deposition in Teflon chambers, Atmospheric Chemistry and Physics, 15, 4197-4214, 2015.

Table S3: Estimated wall loss rates of different dimers

Formula	Volatility range	Used for yield calculation?	k_w (s^{-1})	τ_w (s)	τ_{dil} (s)
$C_{10}H_{16}N_2O_8$	SVOC	No	1.59E-05	8.67E+04	7.2E+04
$C_{10}H_{16}N_2O_9$	SVOC	No	2.99E-05	4.62E+04	7.2E+04
$C_{10}H_{16}N_2O_{10}$	LVOC	Yes	4.57E-05	2.82E+04	7.2E+04
$C_{10}H_{16}N_2O_{11}$	LVOC	Yes	7.76E-05	1.31E+04	7.2E+04
$C_{10}H_{16}N_2O_{12}$	LVOC	Yes	1.12E-04	8.30E+03	7.2E+04
$C_{10}H_{16}N_2O_{13}$	ELVOC	Yes	2.02E-04	3.18E+03	7.2E+04
$C_{10}H_{17}N_3O_{12}$	LVOC	Yes	6.62E-05	3.63E+04	7.2E+04
$C_{10}H_{17}N_3O_{13}$	LVOC	Yes	1.33E-04	1.10E+04	7.2E+04
$C_{10}H_{17}N_3O_{14}$	ELVOC	Yes	1.87E-04	7.96E+03	7.2E+04
$C_{10}H_{17}N_3O_{15}$	ELVOC	Yes	3.61E-04	2.03E+03	7.2E+04
$C_{10}H_{17}N_3O_{16}$	ELVOC	Yes	5.25E-04	1.10E+03	7.2E+04

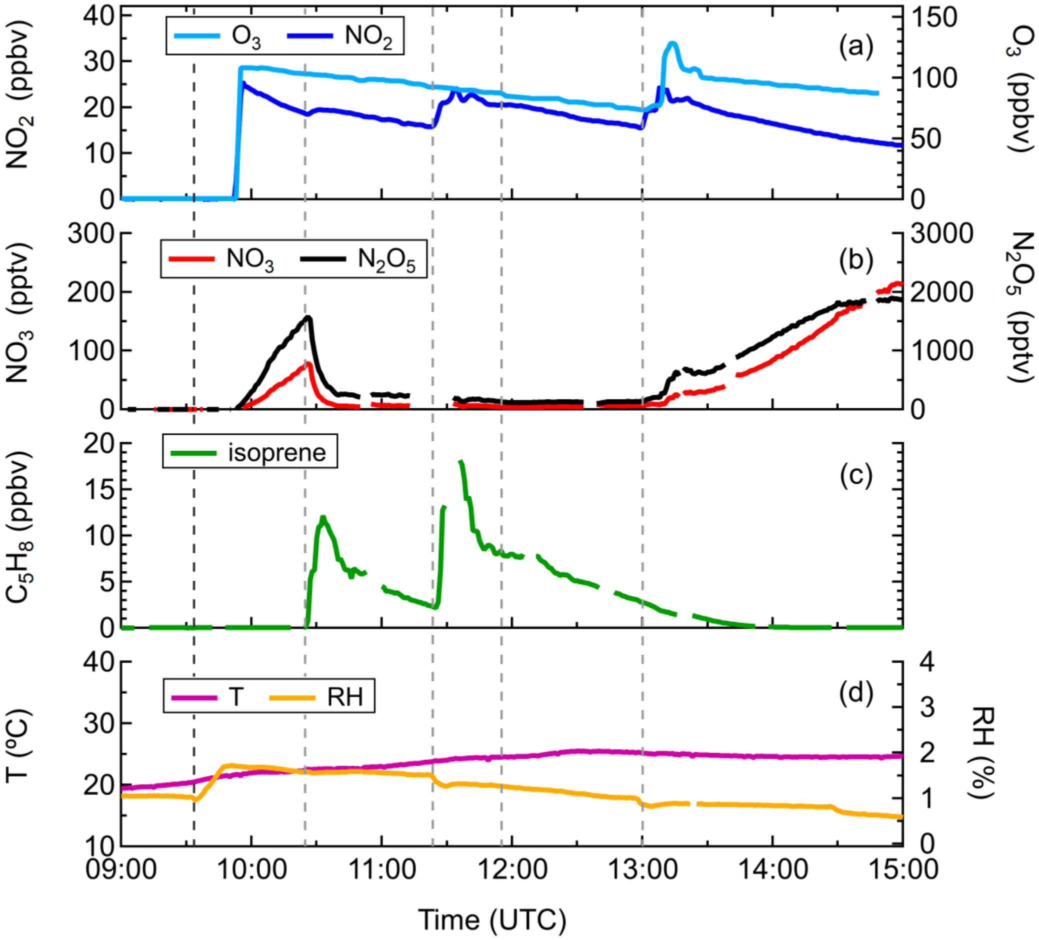

Figure S1: Measurements of (a) O_3 and NO_2, (b) NO_3 and N_2O_5, (c) isoprene and (d) temperature and relative humidity in the chamber during the experiment on 14 August, 2018.

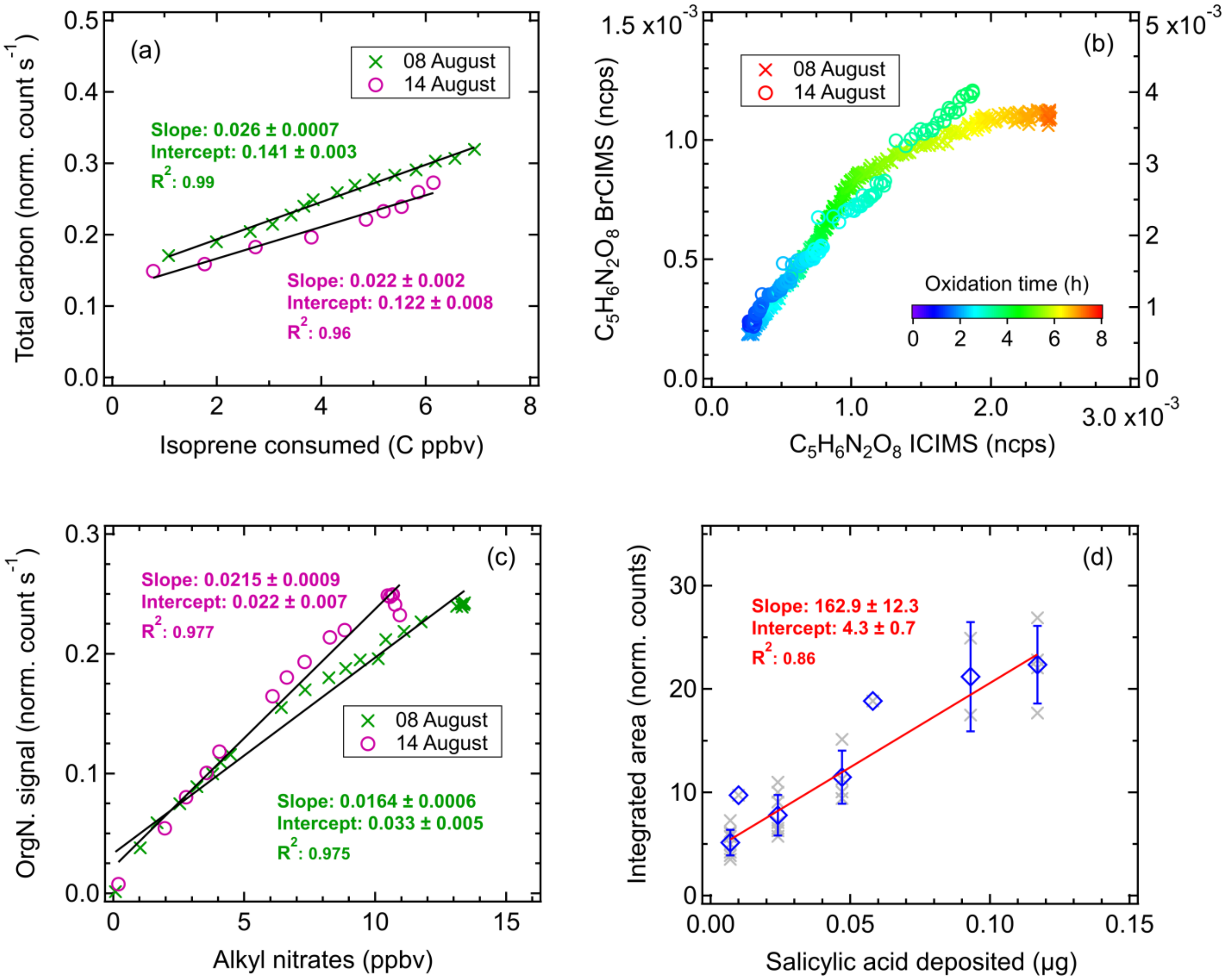

Figure S2: (a) Total carbon detected by Br$^-$-CIMS versus isoprene consumed on 08 and 14 August, 2018. The sensitivity of CIMS for total carbon is determined by the slope of linear fit. The data have been corrected for dilution and wall losses. (b) Comparison of $C_5H_6N_2O_8$ measurements by Br$^-$ CIMS and I$^-$ CIMS. (c) Organonitrates measured by Br$^-$ CIMS plotted against gas-phase alkyl nitrates measured by TDCRDS. The bulk sensitivity for organonitrates is determined by the slope of linear fit. (d) Calibration results of Br$^-$ CIMS for salicylic acid.

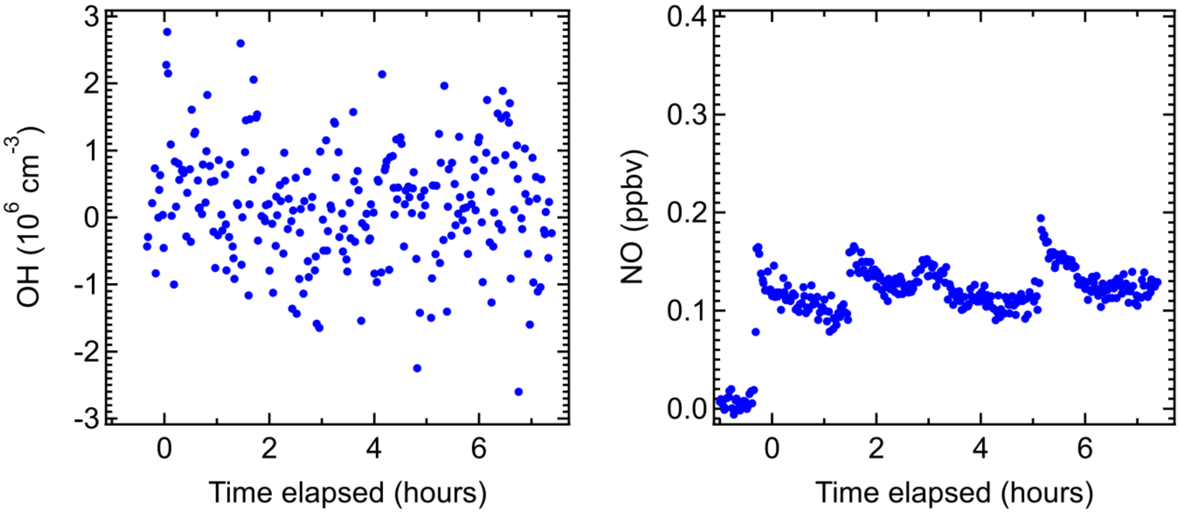

Figure S3: Concentrations of OH radical and NO during the isoprene-NO_3 experiment on 08 August, 2018. The OH concentration was measured by a laser-induced fluorescence (LIF) spectroscopy, and the NO mixing ratio was detected by a chemiluminescence analyzer. It should be pointed out that there was no NO in the chamber, because the lifetime of NO would be very short under high O_3 condition. The non-zero values of NO are measurement artefacts due to the relatively high NO_2 concentration. In addition, the detection limit of NO measurement is higher than 200 pptv.

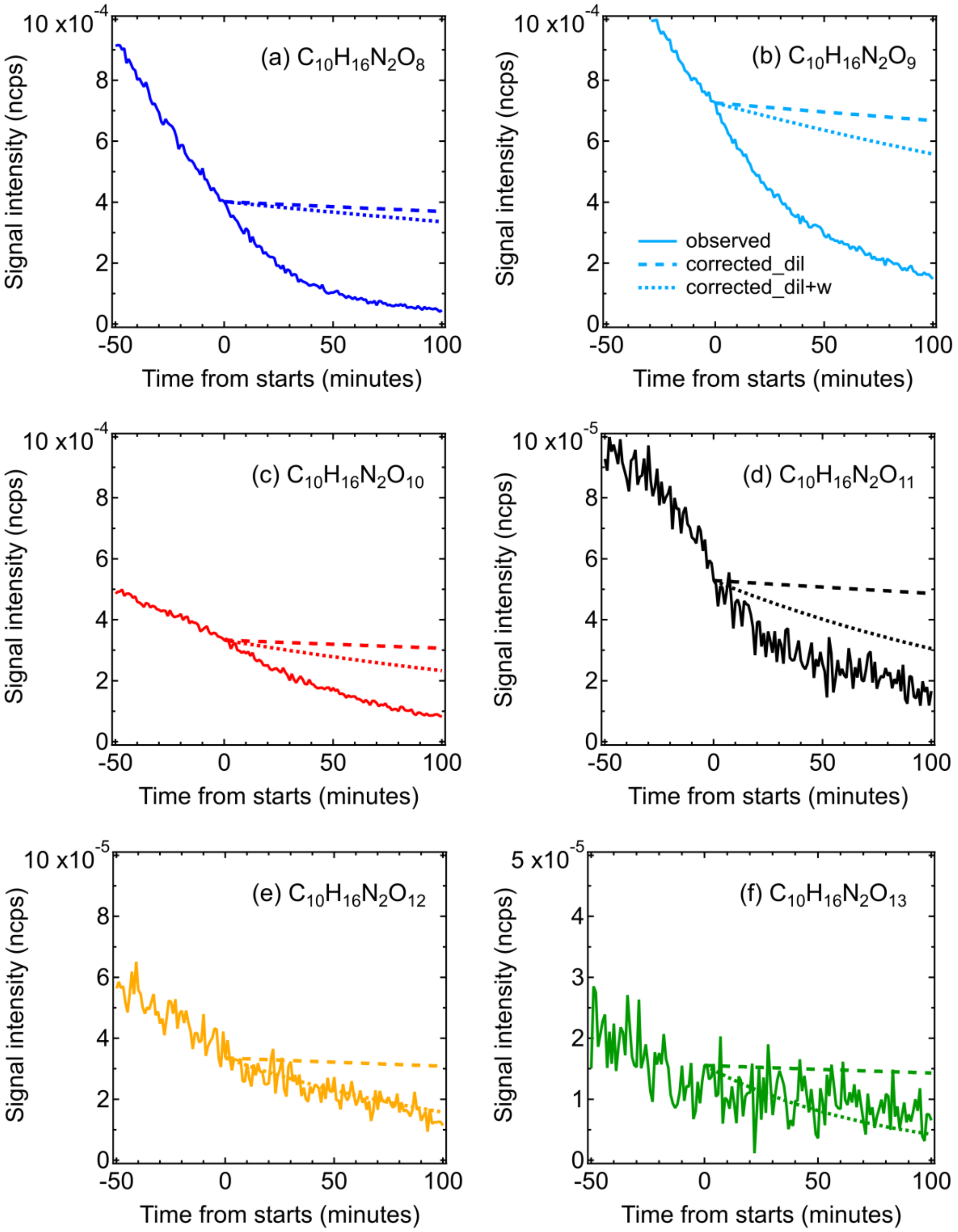

Figure S4: Comparison of the observed and predicted time evolution of 2N-dimers in step IV (only dilution or dilution and wall losses was considered). The time when the last injection of O_3 and NO_2 (without isoprene) occurred is set as zero.

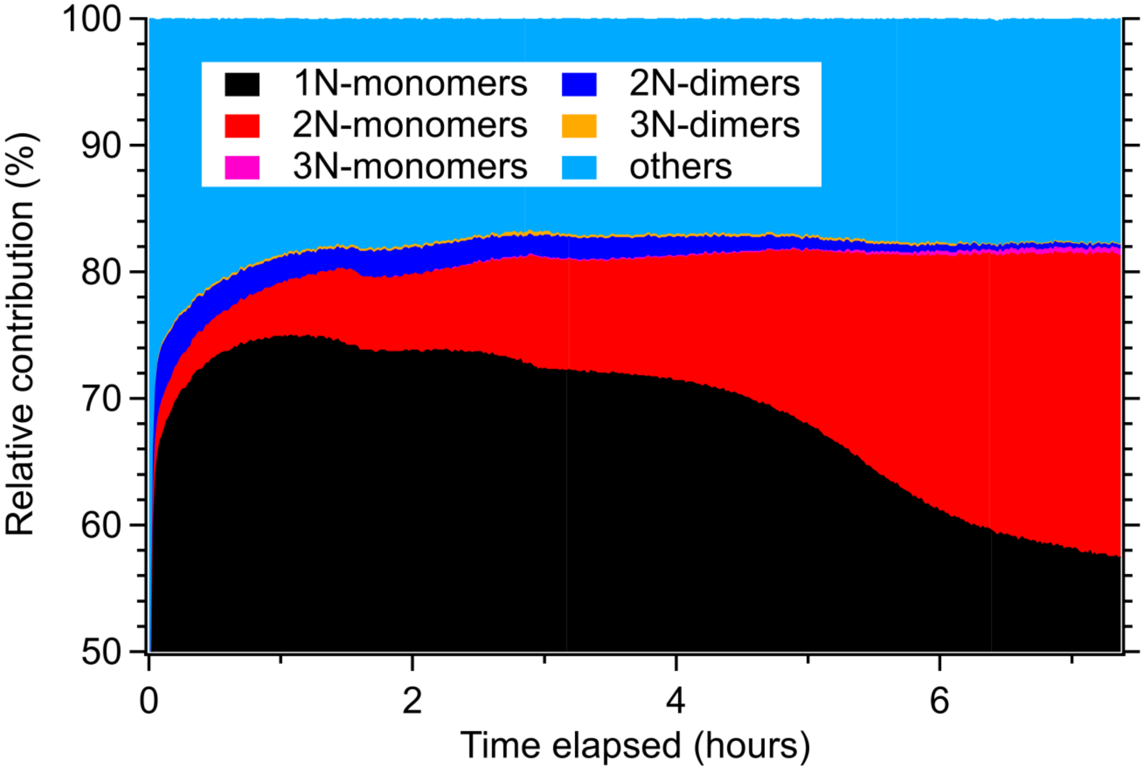

Figure S5: Time evolution of the relative contributions of different chemical groups measured by Br$^-$-CIMS (only organic ions were counted for analysis). 'Others' refers to CHO compounds without containing nitrogen atoms (e.g., $C_5H_8O_2$ and $C_5H_8O_3$).

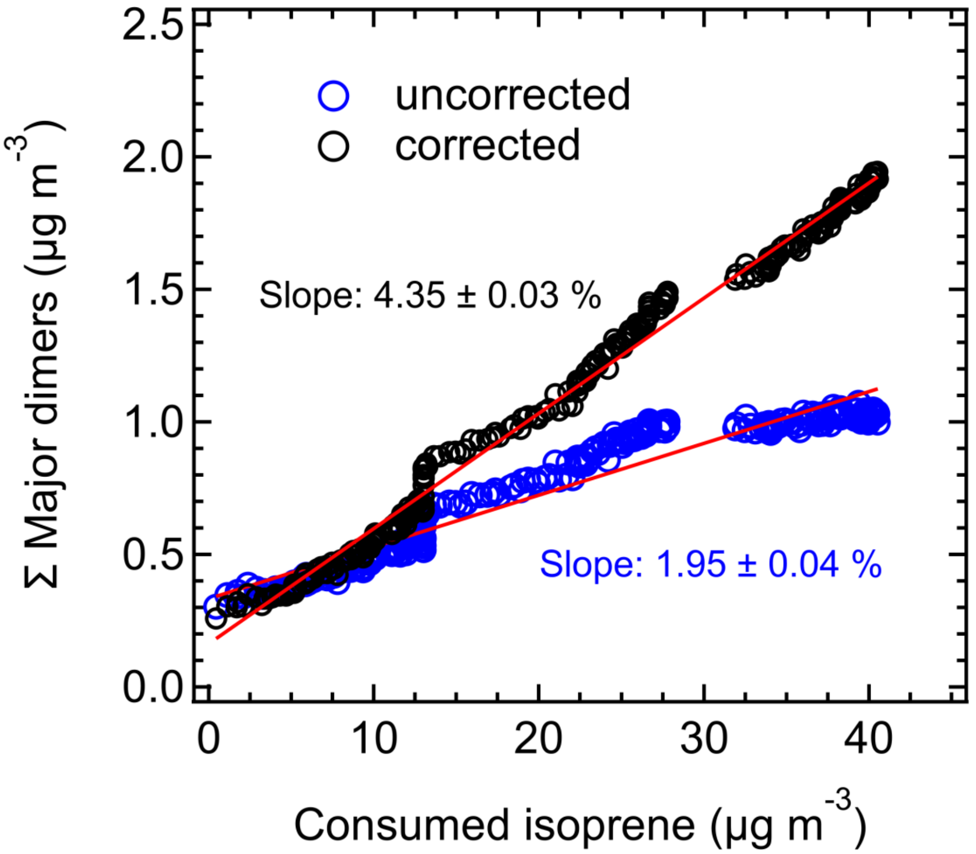

Figure S6: Major dimers mass as a function of consumed isoprene. Fitting a straight line to the data yields slopes of 1.95 ± 0.04 % and 4.35 ± 0.03 % for the uncorrected data and wall and dilution corrected data, respectively. The errors are the statistical errors of the fits. Wall loss corrections are shown in Table S3. Assuming all the dimers in the LVOC and ELVOC range can condense onto particles, producing SOA, we estimate a mass yield of about 5% ± 1.6 %. The relative uncertainty of SOA yield here was estimated to be 32% by using error propagation, which includes the uncertainty of the isoprene consumption concentration (~ 10%), the uncertainty of the alkyl nitrate concentration (~ 10%), the uncertainty of dimer content (~ 20%), and the uncertainty of estimated instrument sensitivity for organonitrates (~ 22%).

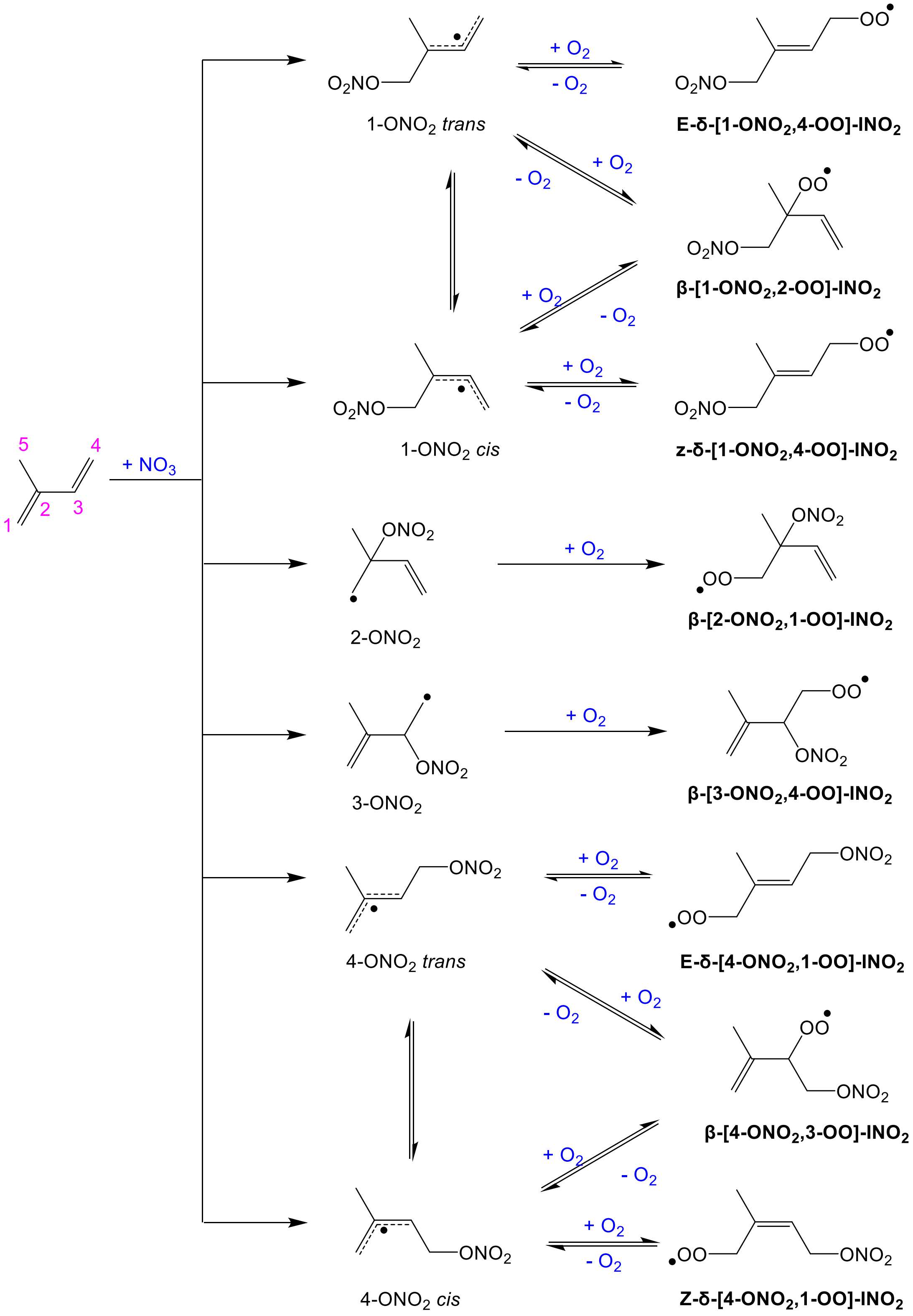

Scheme S1: Formation of isoprene nitrooxy peroxy radicals (INO$_2$) from NO$_3$-initiated oxidation with subsequent O$_2$ addition.

Scheme S2 – S4 serve to show which formula species can be expected in principle accoridng to the understanding of peroxy and alkoxy chemistry under consideration of intramolecular H-shifts and autoxoidation processes.

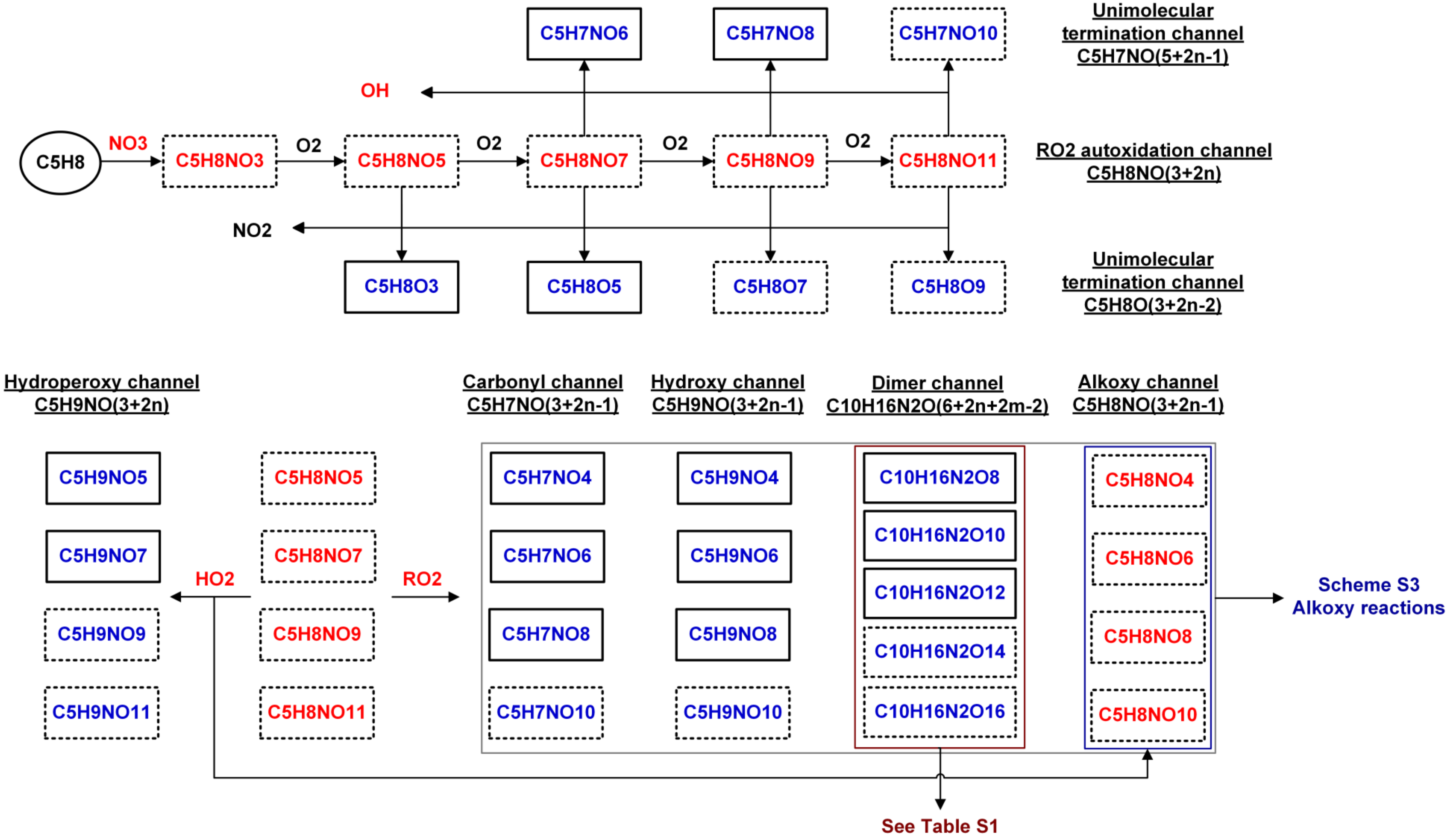

Scheme S2. Proposed first-generation reaction pathways of isoprene-NO_3 and the corresponding products. (n ≥ 1, number of autoxidation steps). Closed-shell products are presented in blue, while radicals are presented in red. Compounds with the given molecular formula in solid boxes have been detected by Br^- CIMS during the experiments, while those in dashed boxes have not.

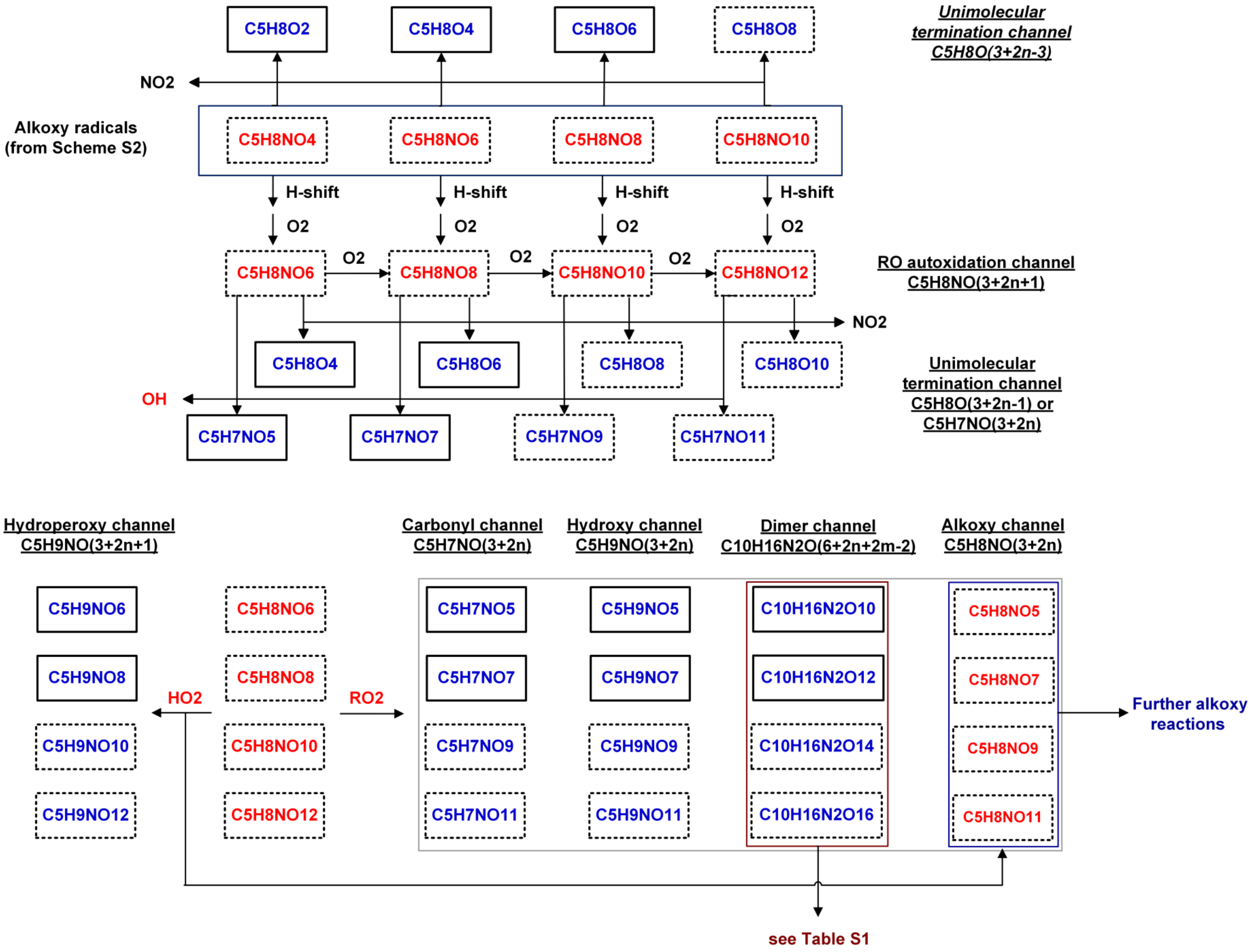

Scheme S3: Proposed reaction pathways of alkoxy radicals (formed from RO_2 alkoxy channel) and the corresponding products (n ≥ 1, number of autoxidation steps). Closed-shell products are presented in blue, while radicals are presented in red. Compounds with the given molecular formula in solid boxes have been detected by Br^- CIMS during the experiments, while those in dashed boxes have not.

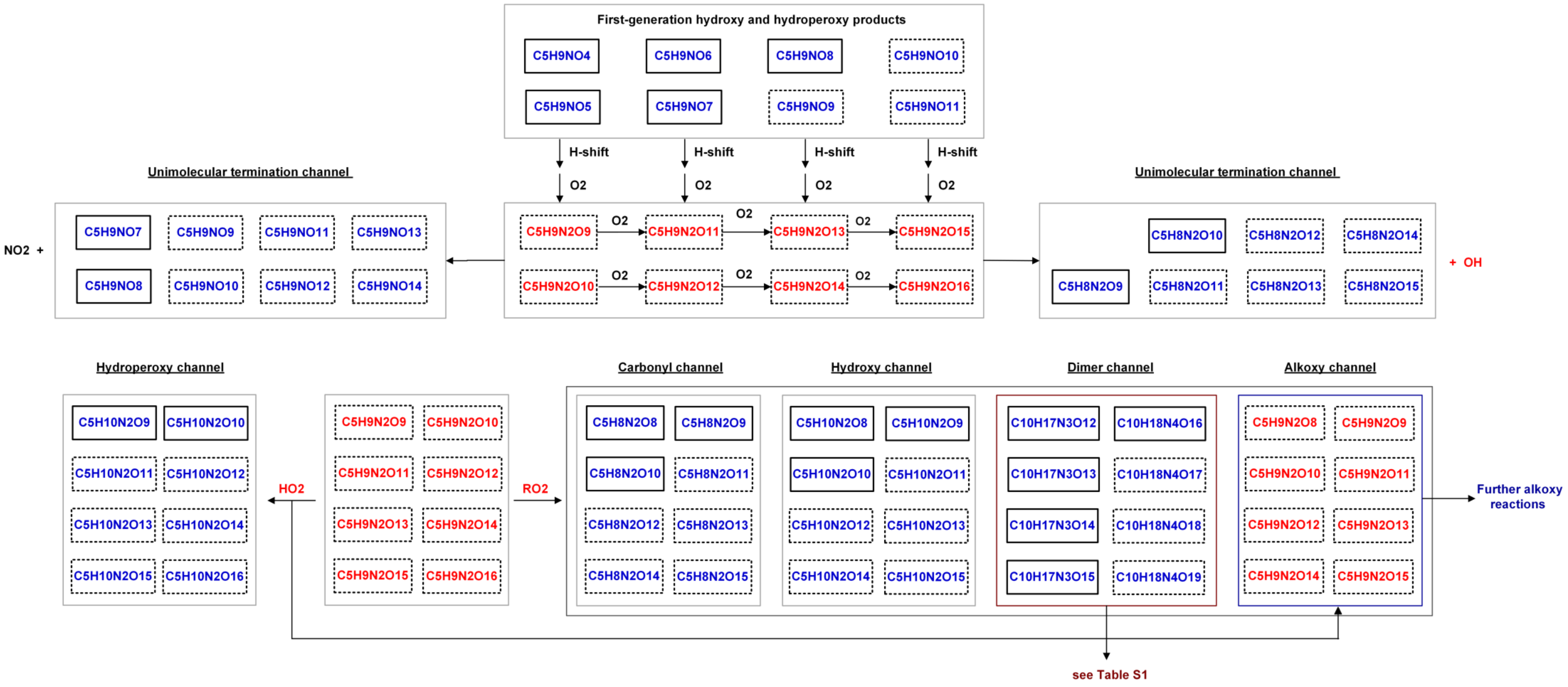

Scheme S4: Proposed second-generation reaction pathways of isoprene-NO_3 and the corresponding products. The subsequent reactions of alkoxy radicals formed in this process are similar to those shown in Scheme S4, therefore not treated further here. Closed-shell products are presented in blue, while radicals are presented in red. Compounds with the given molecular formula in solid boxes have been detected by Br^- CIMS during the experiments, while those in dashed boxes have not.

Scheme S5–S13 are exemplified realizations of reaction pathways shown in Scheme S2–S4 with the purpose to assess possible functionalities of compounds with the given molecular formula. They are used to calculate the range of vapor pressures covered by the observed formula compounds.

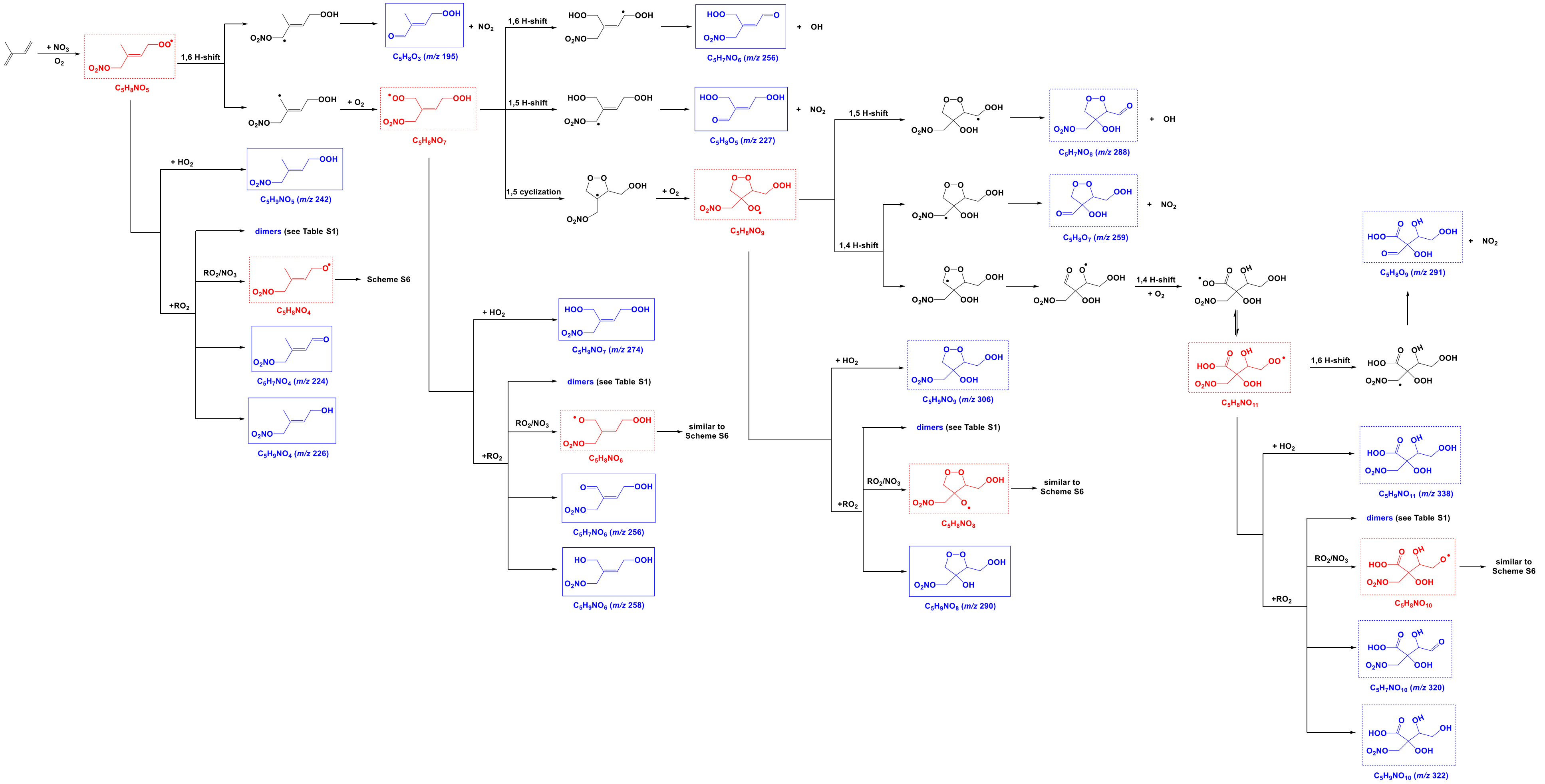

Scheme S5: General reactions and major gas-phase products formed following addition of NO_3 to isoprene. Only one situation is presented, so other isomers are possible. Compounds in blue are the major closed-shell products formed during the reaction, while those in red are major intermediates. Compounds with the given molecular formula in solid boxes have been detected by CIMS as Br^- adducts at the indicated *m/z* values, while those in dashed boxes have not.

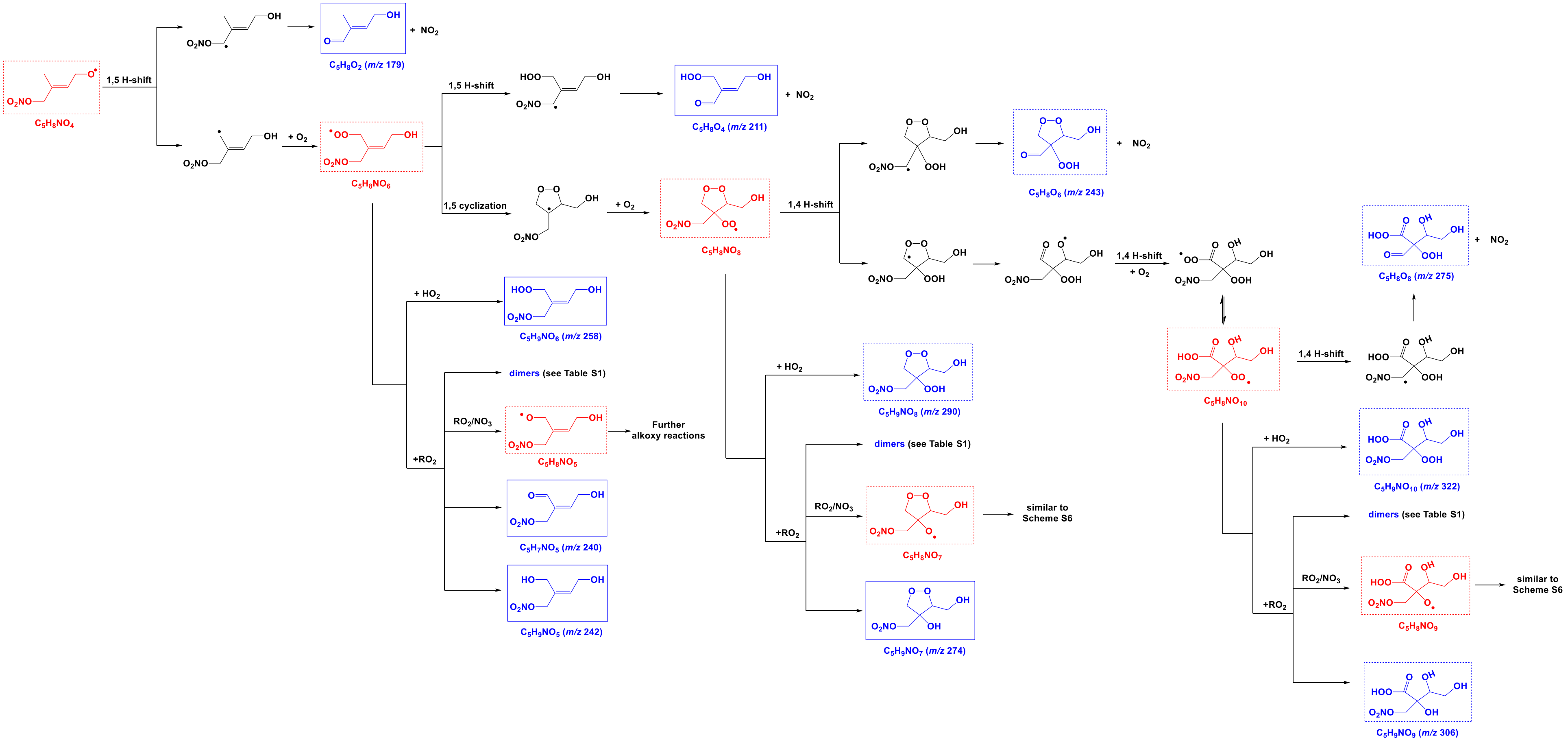

Scheme S6: General reactions and major products formed from rearrangement (H-shift) of the C_5 δ-[1,4]-nitrooxy alkoxy radical. Other isomers are possible. Compounds in blue are the major closed-shell products formed during the reaction, while those in red are major intermediates. Compounds with the given molecular formula in solid boxes have been detected by CIMS as Br^- adducts at the indicated *m/z* values, while those in dashed boxes have not.

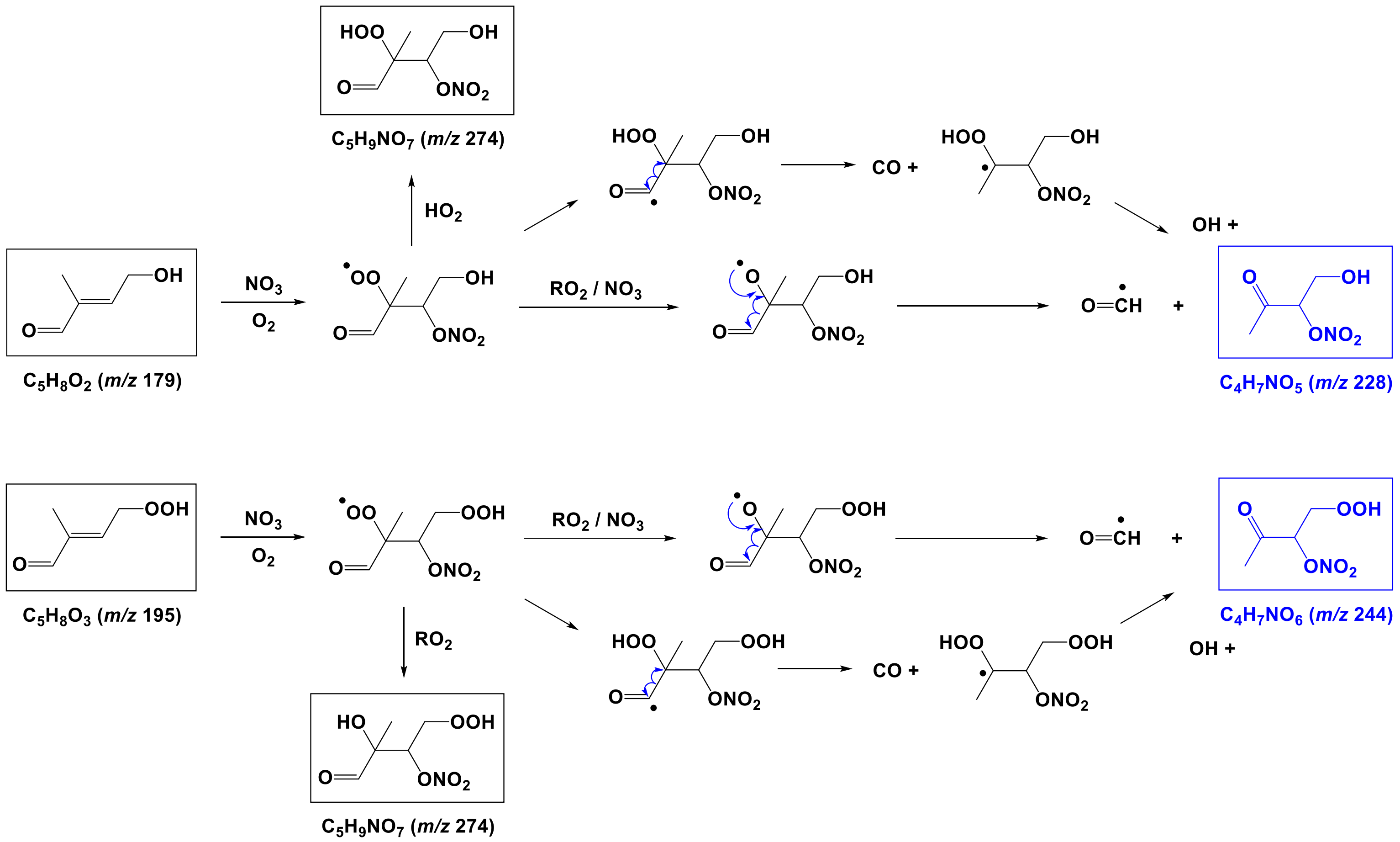

Scheme S7: Proposed formation mechanism of C_4 carbonyl nitrates ($C_4H_7NO_5$ and $C_4H_7NO_6$) from further oxidation of first-generation C_5 carbonyl products. Other isomers are possible. Compounds with the given molecular formula in boxes are closed-shell products detected by CIMS at the indicated *m/z* values.

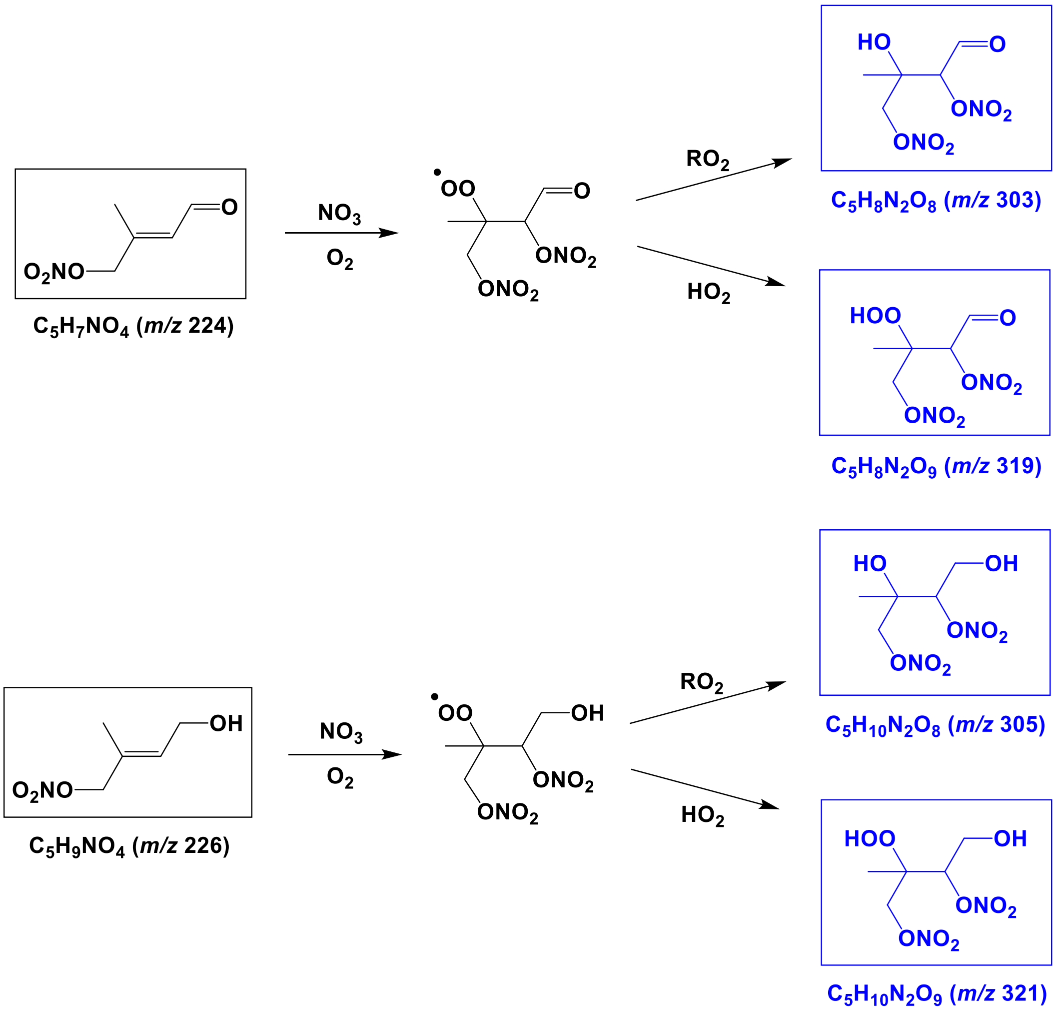

Scheme S8: Proposed formation mechanism of second-generation C_5 dinitrates. Here the major compounds $C_5H_{8,10}N_2O_{8,9}$ are taken as examples for illustration. Other isomers are possible. Compounds with the given molecular formula in boxes are closed-shell products detected by CIMS at the indicated m/z values.

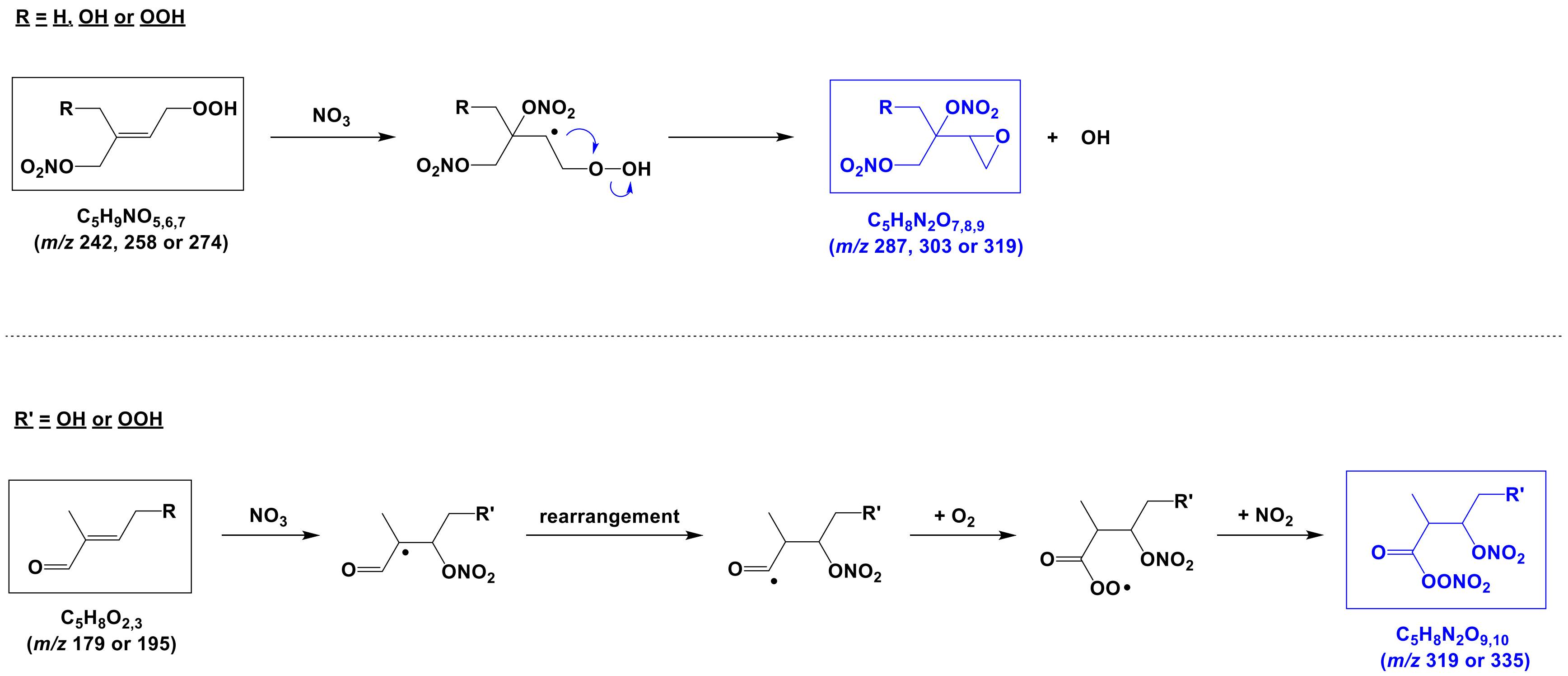

Scheme S9: Proposed formation of dinitrooxy epoxides (upper panel) and petroxyacetyl nitrates (lower panel) from second-generation oxidation by NO_3 with subsequent rearrangement. Other isomers are possible. Compounds with the given molecular formula in boxes are closed-shell products detected by CIMS at the indicated m/z values.

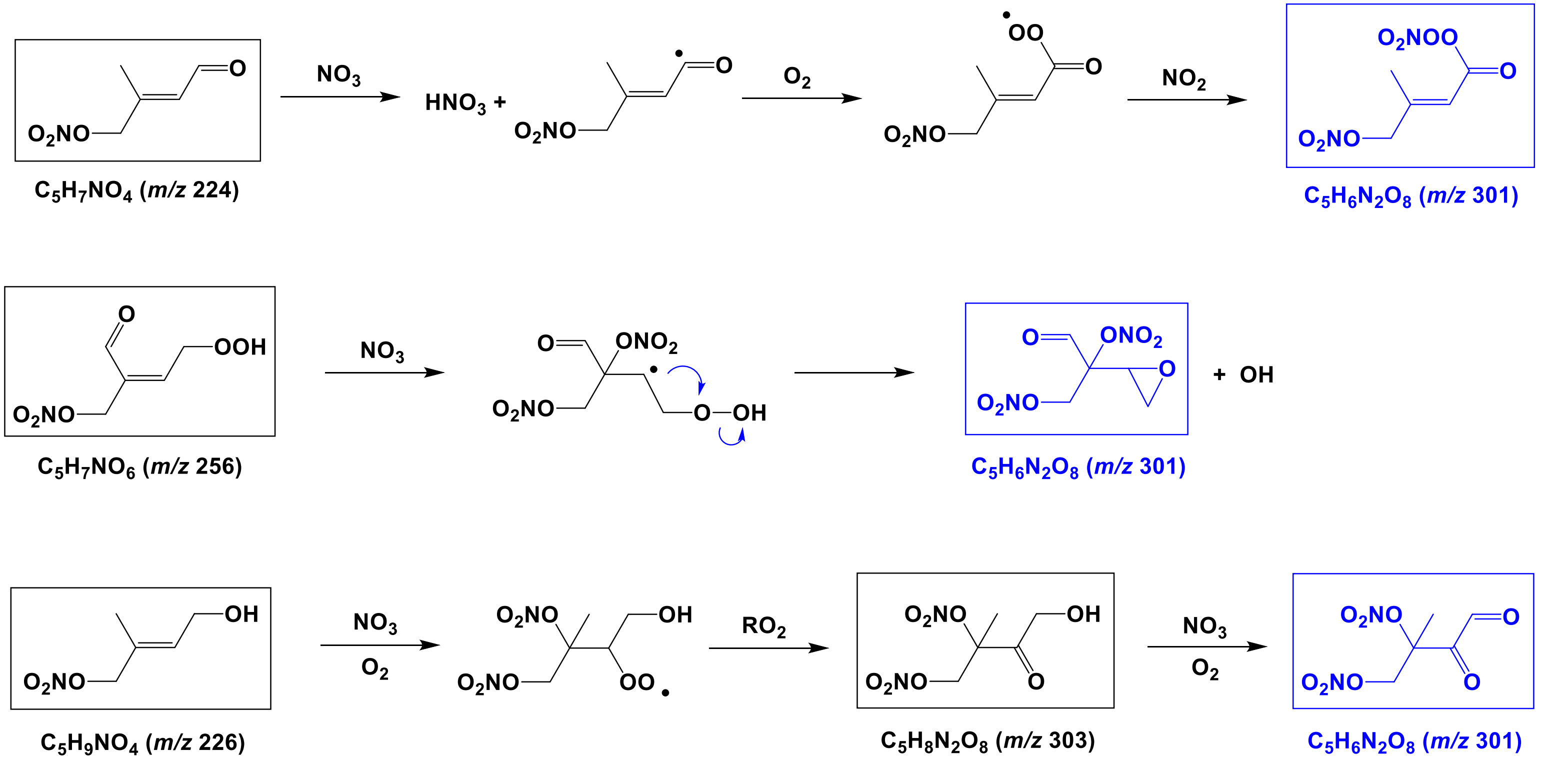

Scheme S10: Possible formation pathways of $C_5H_6N_2O_8$. Other isomers are possible. H-abstraction channel is adapted from MCM v3.3.1. Compounds with the given molecular formula in boxes are closed-shell products detected by CIMS at the indicated m/z values.

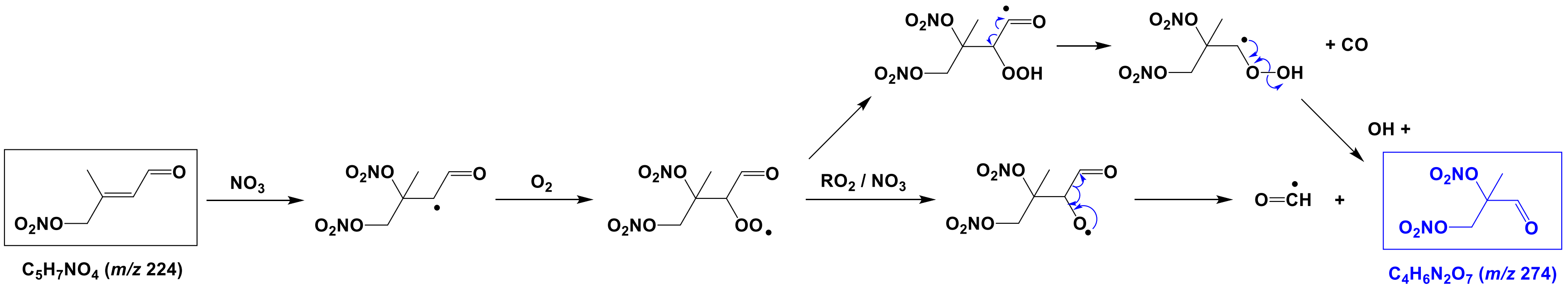

Scheme S11: Possible formation pathways of $C_4H_6N_2O_7$. Other isomers are possible. Compounds with the given molecular formula in boxes are closed-shell products detected by CIMS at the indicated m/z values.

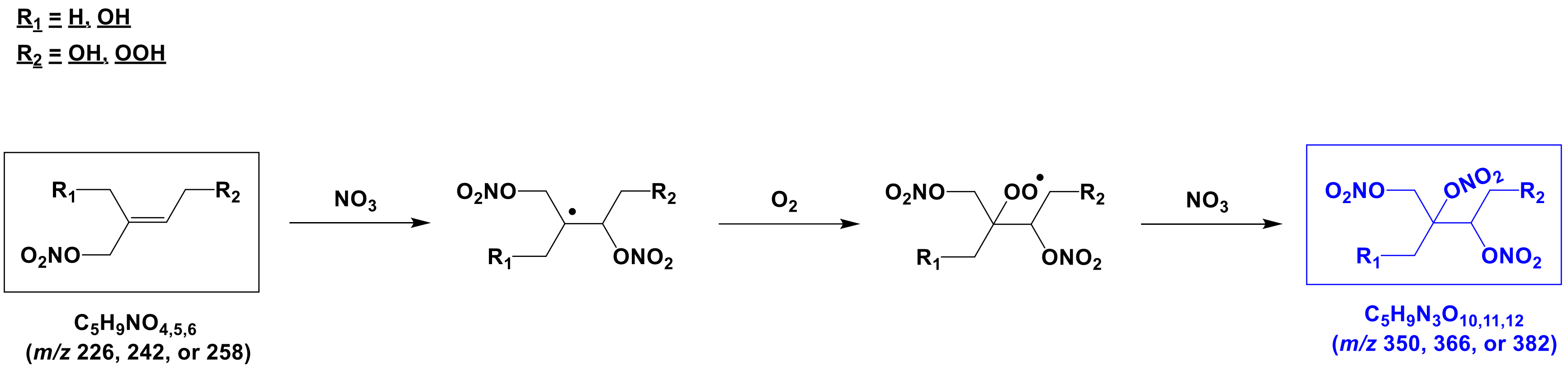

Scheme S12: Formation of trinitrates through further oxidation of the first-generation products by NO_3. Other isomers are possible. Compounds with the given molecular formula in boxes are closed-shell products detected by CIMS at the indicated m/z values.

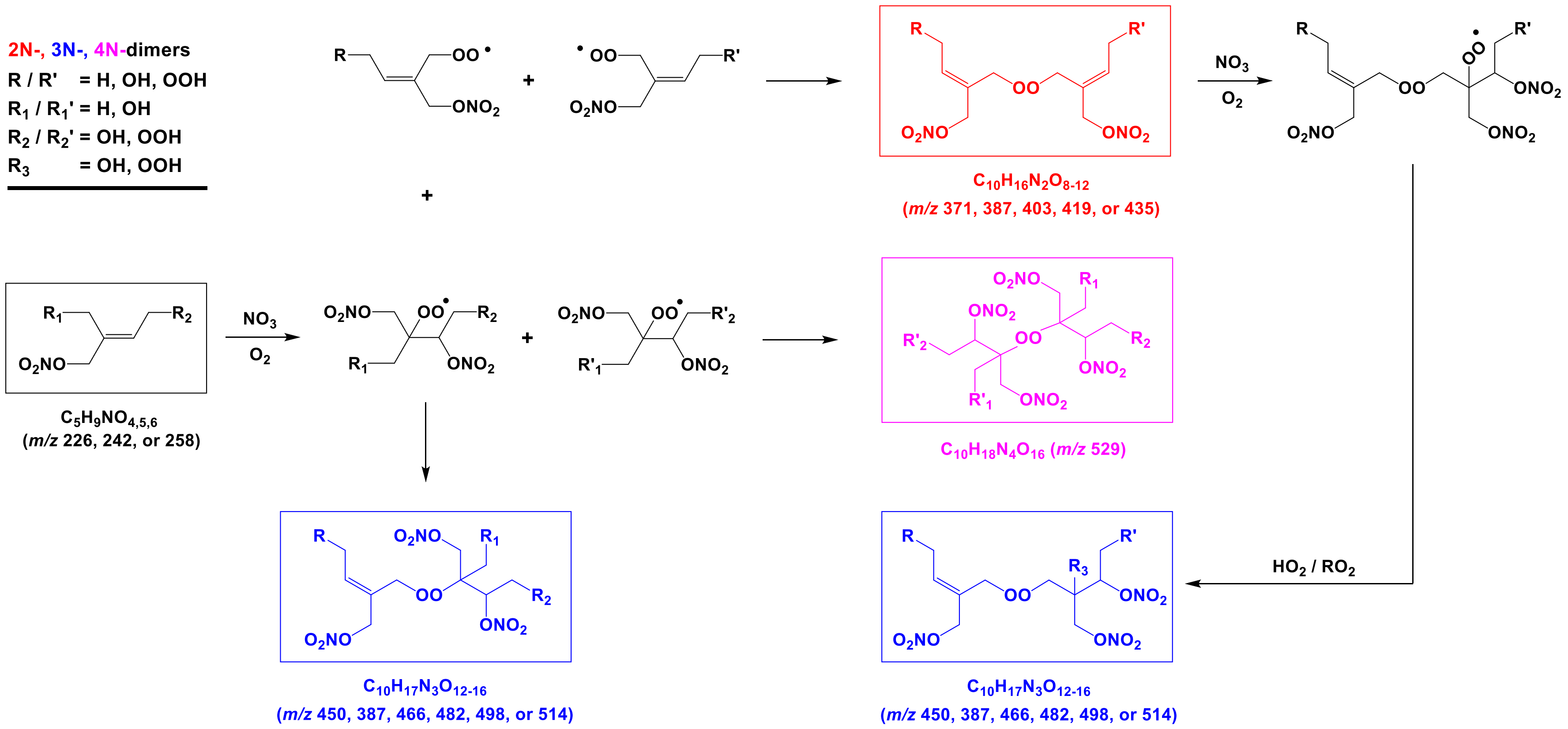

Scheme S13: Proposed formation schematic of different types of dimers (colored by type) through $RO_2 + R'O_2$ reaction or further oxidation. Other isomers are possible. Compounds with the given molecular formula in boxes are closed-shell products detected by CIMS at the indicated m/z values.